Frequency domain signal analysis based index for expulsion quantification in resistance spot welding

Frequency domain signal analysis based index for expulsion quantification in resistance spot welding

Gabriel Antal[1*], Valentino Razza[1] and Manuela De Maddis[1]

[1*]Department of Management and Production Engineering, Politecnico di Torino, Corso Duca degli Abruzzi 24, Torino, 10129, Italy.

*Corresponding author(s). E-mail(s): gabriel.antal@polito.it;
Contributing authors: valentino.razza@polito.it;
manuela.demaddis@polito.it;

Abstract

Resistance spot welding (RSW) is a widespread technique for joining sheet metals. In industrial applications, working closely to expulsion conditions is common practice to maximize the welding size and, thus, the mechanical performance. On the other hand, expulsions lead to the worsening of mechanical characteristics, and the joint becomes visually unappealing. Manufacturing disturbance is another source of expulsion. Abnormal conditions like initial gap and edge proximity are one of the reasons for defects in mass production. This work proposes a procedure to quantify expulsion in RSW through an innovative index obtained from frequency domain analysis of the force signals acquired during the welding process. Furthermore, an indicator extracted from the displacement signals has been compared to the suggested expulsion index. An important finding of this study is that the presented index, in addition to identifying expulsion, indicates how close the process is to the expulsion limit, providing the possibility of recognizing possible shifts and trends that could arise from the actual process conditions. This leads to an effective tool for online process monitoring. Data from an experimental campaign performed to reproduce expulsion in case of inappropriate choice of process parameters, initial gap, and edge proximity validate the effectiveness of the proposed technique.

Keywords: Resistance spot welding, Monitoring index, Expulsion, Frequency domain, Discrete Fourier transform

1

1 Introduction

Resistance spot welding is one of the oldest and most popular fusion welding processes because of its simplicity of usage, low cost, and great efficiency [1, 2, 3, 4, 5]. It consists of joining two or more metal sheets together by applying high pressure and a large electrical current through a couple of electrodes to exploit the Joule effect and form the so-called weld nugget between the sheets. RSW founds large applications, especially in automotive industry, where a single car body contains thousands of spot welds [6, 7, 8].

The spot welding process, like all welding processes, is intrinsically complex. The process design focuses on optimizing the process parameters. However, the actual process may deviate from the expected nominal behavior due to numerous variables. Various factors, including the electrodes (e.g., misalignment, degradation), the welding machine, and the materials themselves can lead to the appearance of defects such as expulsion, porosity, and cracks, as well as different failure modes during the welding process. Therefore, continuous monitoring is essential to preserve high production quality [9, 10]. The ejection of liquid metal during the welding process, known as expulsion, spatter, or flash, is the clearest indicator of process instability and any possible weakness in the produced weld.

By collecting welding process signals, e.g., electrode displacement, dynamic resistance, and applied electrode force, a suitable analysis can detect online the expulsion occurrence [7, 11, 12, 13]. When expulsion happens during welding, some of these signals show specific trends. For example, the displacement and dynamic resistance signals are affected by a sudden decline while, the force one, shows rapid fluctuations [11, 14, 15, 16].

The ISO standard 17677-1-2021 [17] defines the phenomenon of ejected molten metal particles, identifying two possibilities. Expulsions may occur at the faying surfaces of the workpieces (i.e., the surface of a sheet in contact with the other sheet to which it is to be joined) or at the contact interface between the sheet and the electrode during the welding process. The first type of expulsion is highly undesired, as it causes liquid metal to flow out of the nugget during welding, negatively impacting the weld quality. In fact, the molten metal involved in the expulsion is part of the material that was supposed to form the weld nugget but was expelled instead [18]. On the other hand, surface quality and electrode life may be impacted in the second scenario. Accordingly, defects like porosities inside the nugget or excessive indentation may form in the event of a substantial ejection, significantly weakening the weld quality in terms of peak load and energy absorption [19].

Ejections are not only the result of process variability but are sometimes due to an incorrect welding strategy. The typical industrial procedure usually involves process parameters near the condition in which the expulsion occurs, such as a high welding current, to produce large weld nuggets that ensure adequate fusion in the joint and fulfill welding quality requirements.

Besides the incorrect process design, another cause of expulsion arises from manufacturing disturbances. Abnormal conditions like initial gap and edge proximity welding are common reasons for expulsion and low-quality weldments in mass production lines. Previous studies confirm that these disturbances increase the probability of expulsion

and lead to non-satisfactory heat input, producing smaller nuggets [20, 21]. Therefore, it is necessary to prevent expulsion in RSW to solve the issue of unsatisfactory and nonconforming welds. Monitoring and regulating the expulsion phenomenon is essential to modifying welding conditions and lowering the likelihood of this kind of weld strength process fault.

Many efforts have been made to offer solutions: Farson et al. have monitored expulsion in small-scale RSW by measuring the voltage, displacement, and force signals [22]. In [16], Ma et al. study the correlation of dynamic resistance, electrode force, and electrode displacement with the expulsion phenomenon. Xia et al. use the same signals, adding a high-speed camera to explore the relationship between signals and expulsion, and then, they perform linear regression to assess the correlation with the amount of expelled metal, proposing a quantitative evaluation of expulsion [11]. The utilization of a high-speed camera has been performed even by Mikno et al. to determine the most effective signal to find out expulsion (i.e., the force signal), focusing on the possibility of eliminating the issue by stopping the current just before it happens [23]. Other examples can be found either in [24], where Fan et al. determine the different conditions that lead to expulsion by using the dynamic resistance signal, or in [25], in which Kim et al. propose regression models to assess RSW quality criteria, including the presence of expulsion, exploiting features extracted from the welded materials information, displacement and resistance curves. Machine learning (ML) is another widespread tool for quality monitoring in RSW. Regarding this, Podržaj et al. propose a linear vector quantization (LVQ) neural network in [7] to identify expulsion. More recently, Zhou et al. have applied ML methods to monitor the existence of expulsion using the dynamic resistance curves of thousands of spot welds in [26], while, in [27], Russell et al. compare a multilayer perceptron and a convolution neural network for RSW quality criteria prediction, among which expulsion. Yang et al. have exploited the dynamic resistance curves to determine, through different classification algorithms, the quality of spot welds [28]. Random forest-based classification using the same signal is presented by Xing et al. in [14]. Integrating features extracted from process signals and the melting phase of the coating's layer, Kershaw et al. have introduced a model for expulsion detection and RSW monitoring [9].

Mostly, feature extraction related to time domain analysis is performed to assess the presence of either expulsion or other weld defects in RSW. Although it is a common practice for many manufacturing processes [29, 30, 31, 32], frequency domain analysis is less conventional when dealing with RSW signals gained from machine-embedded sensors. In the literature, there are a few examples. Lee et al. [6] have worked on the resistance, voltage, and current signals, decomposed by wavelet transform, to feed ML algorithms for evaluating electrode misalignment. Regarding the expulsion phenomenon, Wu et al. [33] use the same transform, analyzing the force signal to identify expulsion in RSW of titanium alloy, while Chen et al. [34] have applied the wavelet decomposition and a back propagation neural network to determine the presence of expulsion.

This work proposes a novel methodology for expulsion assessment. An expulsion presence index is computed based on the fast Fourier transform (FFT) results on the electrode force signal. Through the FFT, the signal bandwidth is evaluated to detect

fast oscillations in the applied force, detecting the expulsion phase. This approach is computationally cheap and can be easily implemented on the onboard embedded systems to provide real-time feedback to the operator. Moreover, the displacement sensor is exploited to recognize expulsion. Excellent results are achieved in the RSW joints classifications by combining the data analysis from force and displacement signal, leading to 100% positive matches in our experimental campaign. The results show good sensibility in the spatter recognition for the FFT-based analysis, which can highlight changes in welding conditions leading to expulsions. Therefore, it is possible to prevent expulsion in sequence welding by performing suitable maintenance when the expulsion index reaches critical values. This confirms that the force signal offers the most effective way to determine the material ejection, as already verified in [7, 23]. The described procedure gives a straightforward way to identify, in real-time and with very low complexity, either the presence of expulsion and its intensity level or how far the actual working conditions are from the expulsion border. The remainder of the paper is organized as follows. Section 2 discusses the analytical background proposed in this paper. Section 3 describes the experimental setup, while Section 4 shows the experimental results. Conclusions and proposals for future implementation end the paper.

2 Theoretical analysis

2.1 Theoretical behavior of force and displacement curves in the presence of expulsion

According to the literature, e.g., [11, 13, 22, 23, 27], expulsion can be identified by using RSW mechanical signals, such as the force and the displacement signals. The data acquisition is limited to the weld time.
Figure 1 shows the force and displacement signals acquired for two welding points performed, with and without expulsions. Force and displacement are acquired from the RSW machine through a linear position sensor, where the displacement represents the distance between the moving electrode and the fixed electrode, and a strain sensor indirectly measures the force. These green signals (no expulsion) follow a typical behavior due to the physical transformations that the material undergoes during the welding. In the initial phase, i.e., around the first 25 ms of the green curves in Figure 1, the current starts flowing from the electrodes, and the metal sheets begin heating. The higher current intensity is kept for the next 150 ms, leading to the melting of the material, and a larger thermal expansion is observed. Finally, the current ceases, and the metal cools down and shrinks. These thermal effects lead to well-known signal behavior (see, e.g., [15, 18, 35, 36]). The force initially increases due to the slow material expansion (see Figure 1a, green curve), while the electrode displacement remains almost constant (see Figure 1b, green curve). Then, after 25 ms, the thermal expansion is more severe, and the force control produces some oscillations due to the softened metal. Finally, as the metal cools and shrinks, the pressure on the electrodes falls, and the distance between the electrodes reduces.
On the other hand, material expulsion may occur in non-optimal welding conditions. In this case, the welding pool reaches a higher temperature, and part of the liquid

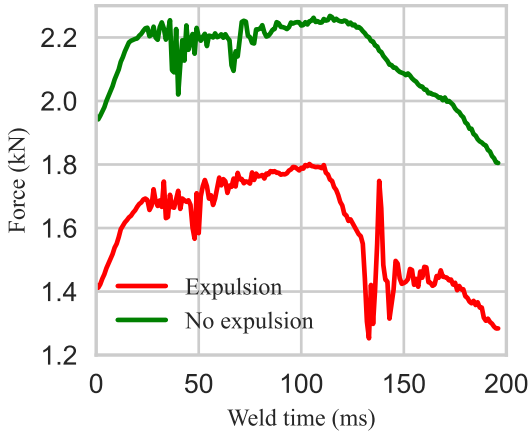

(a) Force behavior.

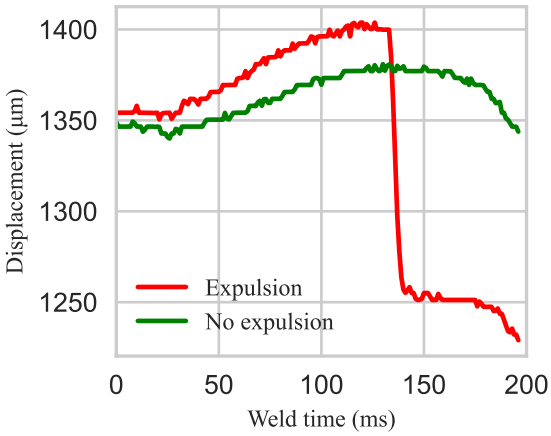

(b) Electrodes distance.

Fig. 1: Signals acquired from the RSW machine for joints with and without expulsions. The force and displacement curves are reported for both welding points.

metal is projected out (see, e.g., [15]). The red curves in Figure 1 show the RSW machine signals acquired in case of expulsions. At the initial phase, the signals are similar to the no-expulsion case. Then, when the metal is projected out, the electrodes lose the support for the lack of material, and the force signal (see Figure 1a, red curve) falls as the metal liquefies. Then, due to the expulsion the electrodes move down (see Figure 1b, red curve) to a new equilibrium.

It is worth noting that, by comparing the curve in Figure 1, in case of expulsion the force signal shows large oscillations, whose amplitude is about 30% the peak value,

in the second half of the weld time, when the metal melts. When the molten material is expelled, the displacement signal suddenly drops, and the electrodes end at a shorter distance than at the beginning of the weld. It is interesting to note that the force signal oscillations precede the displacement drop. Thus, the force signal seems more sensitive in predicting the incoming expulsion.

2.2 Force signal analysis for expulsion detection

In this work, we propose a numerical index to quantify the presence of expulsion in RSW. The *signal bandwidth* is exploited to identify the oscillations previously described from the force signal.
Given the force signal $F(t)$, through the acquisition system, the sampled values $F(k) = F(kT_s)$ are available, where T_s is the sampling period, $k = 0, 1, \ldots, N-1$ is the discrete time index, and N is the number of acquired samples. The discrete Fourier transform (DFT) is defined as

$$\tilde{F}(n) = \sum_{k=0}^{N-1} F(k) e^{-\frac{i2\pi nk}{N}} \in \mathbb{C}, \forall n = 0, \ldots, N-1. \tag{1}$$

The sequence $\tilde{F}(n)$ is the sampled discrete-time Fourier transform of $F(t)$, where the index n is related to a particular frequency through $f = nf_s/N$, having $f_s = 1/T_s$.
For each $n = 0, 1, \ldots, N-1$, a sinusoidal function is defined through the module and phase of the complex number $\tilde{F}(n)$. The sum of all the N sinusoidal functions provides the original signal $F(k)$. In particular, the module of $\tilde{F}(n)$ defines the amplitude of the sinusoidal component. The *bandwidth* of a signal $F(k)$ is defined as a particular frequency f_B such that $|\tilde{F}(n)|$ is negligible for all $n > n_B = Nf_B/f_s$.
Remark 1 *It is worth noting that, in the above definition of bandwidth, we generically state that $|\tilde{F}(n)|$ is sufficiently small or negligible. In fact, due to the presence of the measurement noise, $\tilde{F}(n) \neq 0$ for all $n = 0, 1, \ldots, N-1$.*
A signal having fast dynamic, i.e., large variations in the time domain, is characterized by a large bandwidth. On the other hand, a signal slow in the time domain has a small bandwidth. The interested reader can find details on the DFT and its properties in [37].

For simplicity of notation, we define $X(n) = |\tilde{F}(n)|^2$, and the equivalent value in decibels

$$X_{\mathrm{dB}}(n) = 20 \log_{10} |\tilde{F}(n)|. \tag{2}$$

as the module square of $\tilde{F}(n)$. From the Parceval's theorem (see, e.g., [37]), the following relation holds

$$E = \sum_{k=0}^{N-1} |F(k)|^2 = \sum_{n=0}^{N-1} X(n), \tag{3}$$

where E is the *energy* of $F(k)$. Thus, $X(n)$ assumes the meaning of *energy spectral density* since it describes how the energy of $F(k)$ is distributed along the frequency

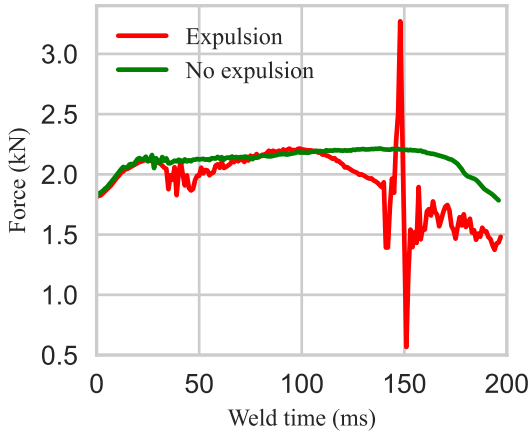

(a) Force behavior in the time domain.

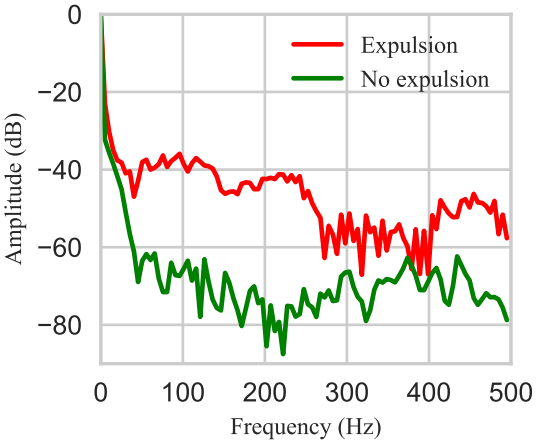

(b) Force energy spectral density in dB.

Fig. 2: Force signal acquired from the RSW machine for joints with and without expulsions. On top are the acquired signals in the time domain, above the normalized energy spectral density.

components. Information equivalent to bandwidth can be retrieved by introducing the *residual energy* as

$$R^{n_x} = \sum_{n=n_x}^{N-1} X(n) \tag{4}$$

7

which is the difference between the signal energy E and the energy spectral density limited to its first n_x values. Residual energy can be expressed in dB as

$$R_{\mathrm{dB}}^{n_x} = \sum_{n=n_x}^{N-1} X(n)_{\mathrm{dB}} \tag{5}$$

Since our objective is to identify the large oscillations in the force signal preceding the expulsion phase, we propose to compare the index R^{n_x} given the force signal acquisition from the welding machine. However, from (1), it is worth noting that a scaling factor c on the force in the time domain scales the DFT $\tilde{F}(n)$ as well. Thus, by defining a signal $F_1(k)$ and its DFT $\tilde{F}_1(n)$, the scaled signal $F_2(k) = cF_1(k)$ leads to $\tilde{F}_2(n) = c\tilde{F}_1(n)$. The scaling also reflects on the index R^{n_x}. Thus, we define

$$\overline{R}^{n_x} = \sum_{n=n_x}^{N-1} \overline{X}(n) \tag{6}$$

where

$$\overline{X}(n) = \frac{|\tilde{F}(n)|^2}{|\tilde{F}(0)|^2}. \tag{7}$$

Figure 2 shows the force signals acquired during the welding process, with and without expulsion, highlighting with different colors the entity of the oscillations to be detected. The normalized energy spectral densities for the two signals are shown in Figure 2b. Through graphical comparison, the signal without expulsion has a smaller bandwidth than the one with expulsion, as expected. While $\overline{X}_{\mathrm{dB}}(n)$ is contained between -80 and -60 dB in case of no spatter, $\overline{X}_{\mathrm{dB}}(n)$ is larger, up to -40 dB, in case of expulsion. The user's choice of the index n_x is arbitrary and should be tuned to adequately adapt to the process.

2.3 Displacement signal analysis for expulsion detection

Like the force signal, the electrode distance provides information on the material expulsion. During a weld without expulsion, the displacement signal is almost constant, with variations of a few micrometers (see Figure 1b, green curve). On the other hand, the lack of support due to the material expulsion leads to a fast electrode distance reduction (see Figure 1b, red curve). Therefore, we propose an index based on the maximum variation of the acquired sampled displacement signal $d(k)$. Since it is not possible to define the derivative function for a discrete-time function, we define the index

$$S = \max_k \frac{|d(k+1) - d(k)|}{T_s} \tag{8}$$

as the maximum difference quotient, representing the maximum electrode relative speed during the welding process. It is worth noting that, given the same acquisition sampling time T_s for all the experiments (see 4.2), (8) can be simplified as

$$S = \max_k |d(k+1) - d(k)| \tag{9}$$

where the maximum of the finite difference is considered.

3 Experimental setup

A medium-frequency direct current RSW machine, working in constant current control mode (CCC) [38], with a TE700 (Tecna) control unit, has been utilized to run the experimental welding operations. This working mode has been chosen to control the input current and avoid one more source of variability. This machine is equipped with a set of sensors to monitor the process. Along with the available sensing devices, in this study, the following have been considered: a piezoelectric surface strain sensor (Kistler Italia, mod. 9232A, sensitivity ≈ -80 pC/$\mu\varepsilon$), to acquire the electrode force during the welding process, and a magnetostrictive linear position sensor (Temposonics R-series, resolution of 2 µm), to measure the electrode displacement. Signals are acquired through a National Instruments cRIO 9035 at a 40 kHz sampling rate. The material used is the GI50/50-U zinc-coated DP590 steel, which is part of a materials category widely utilized in the automotive industry [35, 36]. The thickness of the single sheet is 0.8 mm. According to ISO 14273, [39], the individual test piece dimensions are (45x105) mm, and the weld overlap is 35 mm, as shown in Figure 3. Weldings have been performed with two Cu-Cr-Zr electrodes, having a truncated cone shape and a nominal contact diameter of 4.5 mm, as recommended by ISO 14373 standard [40]. The bottom electrode is fixed while the top electrode moves to clamp the sheet stack. Electrodes cooling is achieved through a water flow of 4 L min^{-1}, as advised by the same standard [40]. The partial weldability lobe at constant welding time has been built per ISO 14327, and ISO 18278-1 [41, 42]. Both standards suggest the lobe lower limit to a weld diameter $w_d = 3.5\sqrt{t}$, where $t = 0.8$ is the material thickness, and the upper limit is the maximum welding conditions before expulsions occur. Welding time-related parameters have been chosen according to ISO 14373 [40]. Following the ISO 17677-1 [17] nomenclature, the weld time is given by the sum of upslope (25 ms), downslope (25 ms), and current time (150 ms). In our experiments, the weld time is set to 200 ms. Focusing on the upper limit, 13 different combinations of welding current $I = \{6.5, 7, 7.5, 8\}$ kA and welding pressure $P = \{0.8, 0.9, 1, 1.1\}$ bar have been chosen to perform 39 spot welds (i.e., 3 welds for each combination). Table 1 summarizes welding parameters. According to ISO 14373 [40], the first points have been made with 7 kA and 1 bar. From the welding machine technical characteristics, the force F pressure P relationship is

$$F = 2.07P. \tag{10}$$

For each spot-welded specimen, a standard testing machine has carried out the shear tension test (STT) with a crosshead speed of 10 mm min^{-1}. Finally, the measure of the weld diameter, i.e., the mean diameter of the fused zone at the faying surface after destructive testing, has been performed employing a digital caliper (see Figure 4b), as recommended by ISO 17677-1 [17].
Through visual inspection, the presence of expulsion has been assessed, and the partial welding lobe (right limit zone) has been built. Figure 4a shows one of the specimens, after the tension test, in which welding has been affected by the presence of expulsion.

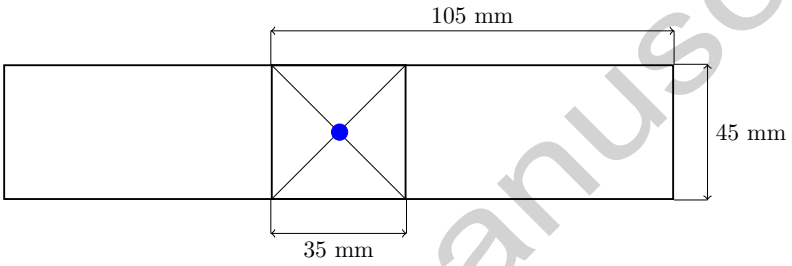

Fig. 3: Specimen geometry according to ISO 14273.

10

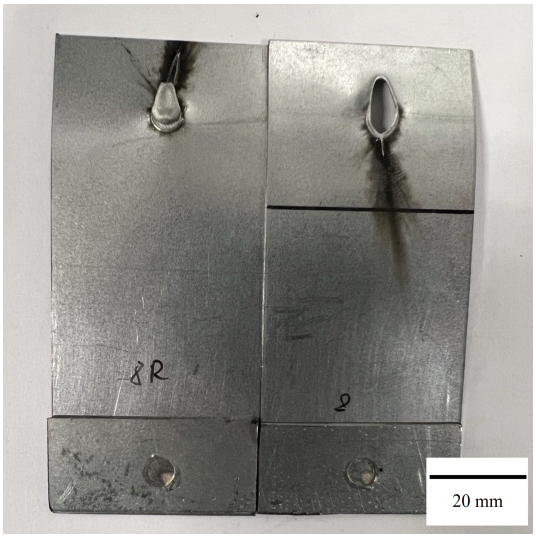

(a) Specimen with expulsion, after shear tension test.

(b) Weld diameter measurement, after shear tension test.

Fig. 4: Expulsion-affected specimen and weld diameter measurement.

4 Results and discussion

4.1 Definition of weldability lobe

Through the experimental setup discussed in the previous section, a total of 39 RSW joints have been initially performed (13 groups, Table 1). Given the results, the partial weldability lobe has been constructed. The average weld diameter and failure peak load are considered for each group. The following rules, based on ISO standards, have been applied to select the compliant joints.

1. If the weld diameter is below $w_d = 3.5\sqrt{t}$ mm, i.e., approximately 3.1 mm for $t = 0.8$ mm, the group is not compliant (see [40]).
2. If the peak load is lower than ISO requirements (in this case 2.3 kN), the group is not compliant (see [40]).
3. If there are no expulsions, the group is compliant (green) (see [41, 42]).
4. If there is only one point with expulsions, the group is partially compliant.
5. If most points are affected by expulsion, the group is not-compliant (see [41, 42]).

The first rule is always satisfied since the welding parameters have been selected to reach the minimum weld size $w_d = 3.1$ mm. The fourth rule is not from ISO standards, and it has been defined to highlight the contour of the weldability lobe as a border between the compliant and not-compliant joints. Figure 5 shows the resulting weldability lobe. The colors have been assigned to highlight the joint categories. The weak joints, i.e., not conforming to rule 2, are in blue. Green and red blocks denote groups with compliant and noncompliant joints, respectively, by ISO standards. In orange are the groups with partially compliant joints.
The experimental data confirm some known relationships (see, e.g., [18]). The peak load is mainly related to the weld diameter, even if the geometrical size is not the only parameter affecting the weld strength.
The weld size is proportional to the input current I. In fact, the energy delivered, and, thus, the welded material, is proportional to the welding current, leading to a larger weld spot. For example, the comparison between weldings in group 4, made with $I = 6.5$ kA, and group 1, made with $I = 7$ kA, shows this relationship. Both groups are characterized by the same welding pressure $P = 1$ bar. The average weld diameter is $w_d = 4.43$ mm in group 4 and $w_d = 4.92$ mm in group 1. A large current value is the main cause of expulsions.
Even if counter-intuitive, increasing electrode pressure P can decrease weld size w_d. This happens due to two competing factors. On the one hand, higher pressure creates a better connection between the electrode and the sheet metal being welded, which reduces the electrical resistance at the contact point, i.e., lowers the heat generation in that area. Heat is what melts the metal and forms the weld nugget. So, with less heat, the weld grows smaller. On the other hand, increased pressure can also squeeze the molten metal at the weld zone outward. This can expel some of the molten material, limiting the overall size of the solidified weld diameter. The comparison between weldings in groups 4 and 10 shows this inverse proportional relationship between pressure P and weld size w_d. While the welding currents are the same, $I = 6.5$ kA, decreasing the pressure from $P = 1$ bar to $P = 0.9$ bar leads to the average weld

diameter changing from $w_d = 4.43$ mm to $w_d = 4.70$ mm, respectively.
Expulsions in RSW are directly related to weld size, specifically the weld diameter. In fact, expulsions are often seen as a sign of an excessively large weld nugget. The experimental data in groups 1, 2, and 3 verify this, where the presence of expulsions is related to larger weld diameters. During RSW, heat generated at the contact point melts the metal, forming the weld nugget. With proper settings, this nugget grows to an ideal diameter for strong bonding. Excessive heat due to improper settings, e.g., high welding current I, may lead to the weld nugget becoming excessively large. Therefore, the molten metal under pressure has nowhere to go and gets squeezed out, forming expulsions around the weld zone [7, 18]. In some applications, a slightly larger weld diameter due to minor expulsions might not be detrimental and could offer a larger peak load. In groups 10 and 11, the welding parameters change, leads to an average increment of the peak load, even if some expulsions occurred. It is worth noting that one out of three tests in group 11 having expulsions reached larger values in STT than joints in the group 10. However, expulsions are essentially molten metal that squeezes out of the weld nugget during the welding process. Moreover, the expulsion process can create cavities or voids around the expelled material. These voids act as stress concentrators, making the weld more susceptible to cracking under shear tensile stress applied during testing. A smaller STT result in the presence of expulsions is seen in the group 6 compared to group 1. In group 1, without expulsions, the average joint peak load is 3.13 kN, and the weld size is 4.92 mm. In group 6, all the joints had expulsions, and, on average, the weld size is larger, $w_d = 5.02$ mm. However, the average peak load decreases to 3.03 kN. Accordingly, expulsions are generally undesirable in RSW applications where strong shear strength is required.

4.2 Data acquisition

Some sensors monitor the welding machine. As described in the previous section, analogic displacement and force sensors are applied to the electrodes, and data is stored through a digital acquisition system. The electromagnetic disturbances from the welding process lead to really noisy data. This noise is a random fluctuation in the signal itself or introduced during the measurement process.
The oversampling technique has been applied to acquired data to mitigate the impact of measurement noise. Oversampling is a valuable tool for reducing the impact of noise when reconstructing signals at a lower frequency than the sampling rate, and it works best for random, zero-mean noise. The original data acquisition frequency is set to 40 kHz. Then, data is split into groups of 40 samples. Only one value, the average, is kept for each group, leading to an effective data acquisition frequency equal to 1 kHz.

4.3 Force and displacement signals analysis

The portion during the weld time (200 ms) is considered among the force signals acquired during the process. For each joint, eq. (6) is applied to compute the residual energy $\overline{R}^{10}_{\mathrm{dB}}$, where $n_x = 10$ is chosen from experimental trial-and-error procedure. It is worth noting that higher residual energy corresponds to a more severe expulsion.

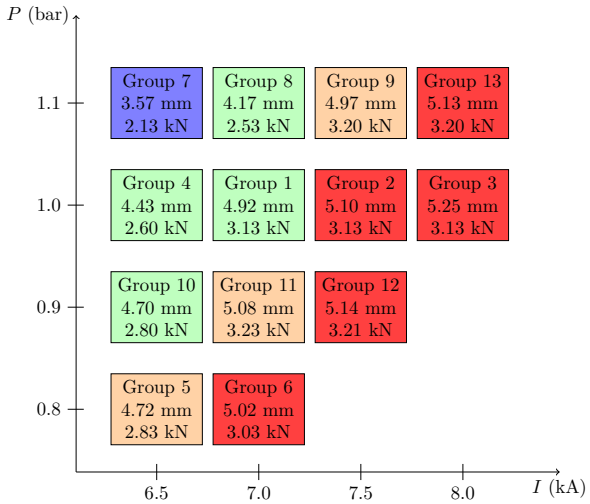

Fig. 5: Weldability lobe. Three test repetitions have been performed for each group. Within the boxes, the average weld diameter and failure load are reported. Colors highlight the welding quality. Low failure loads are denoted in blue. In orange and red are marked groups where expulsions occurred. If one joint in the group had expulsion in orange, two or more in red. In green are the good-quality sample groups.

Figure 6a shows welding points and expulsion compared to their $\overline{R}^{10}_{\mathrm{dB}}$ value. As expected from the process parameters, point number 9, which belongs to group 3, demonstrates a higher intensity of expulsion. The cross-sections of the same specimens can be observed in figure 6b. Weldings 1 and 9 (no expulsion vs high expulsion) have the same input pressure but different welding currents (7 and 8 kA). After the cross-section cut, only one side of the welding nugget remained in the case of number 9. Although after STT both have shown a satisfactory weld diameter (4.95 vs 5.35 mm), a pull-out fracture, and a high peak load (3.2 vs 3 kN), number 9 has a high indentation depth which should be lower than 20% of the thickness, according to ISO standards [40]. This confirms that having a standards-compliant diameter and peak load is insufficient to satisfy all quality requirements. Consequently, considering expulsion is crucial for RSW quality assessment.

Figure 7a shows $\overline{R}^{10}_{\mathrm{dB}}$ for the 39 welding points made. A threshold equal to -5400 dB can be defined to separate joints with and without expulsions. Such a threshold depends on several parameters, e.g., sampling frequency and welding process duration. Thus, the threshold and the weldability lobe definition should be detected experimentally. Moreover, the $\overline{R}^{10}_{\mathrm{dB}}$ value distance from the threshold is smaller as the welding parameters are closer to the expulsion conditions and vice-versa. The joints within the partially compliant groups (marked in orange) are the closest to the threshold. Group 3 is the rightmost in the weldability lobe (see Figure 5) and has the largest $\overline{R}^{10}_{\mathrm{dB}}$. Similarly, joints in group 4, the leftmost group from the non-compliant condition, have the smallest residual energy value.

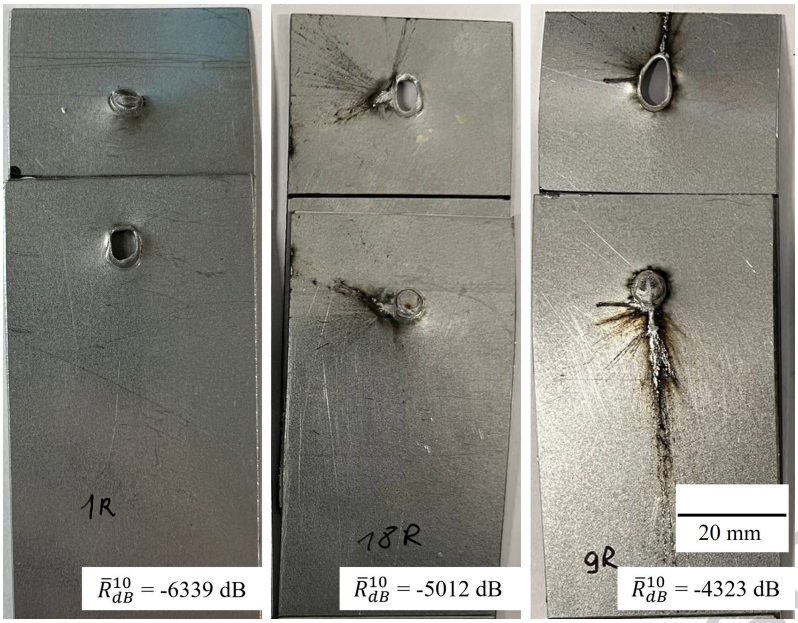

(a) Expulsion severity and $\overline{R}^{10}_{\mathrm{dB}}$ for specimens 1, 18, and 9.

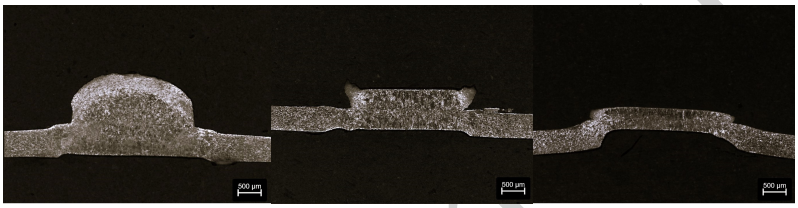

(b) Cross sections, after STT, for points 1, 18, and 9.

Fig. 6: Specimens 1 (group 1, no expulsion), 18 (group 6, medium expulsion), and 9 (group 3, high expulsion).

Through the electrode displacement signal, the expulsions are recognized as well. The S index is computed according to (9) for all the 39 experiments. Just like the index $\overline{R}^{10}_{\mathrm{dB}}$, it is possible to identify a threshold to split the set of joints with or without expulsions. In this case, 15 µm is the threshold value. It can be observed that the expulsion presence is always recognized, but the behavior is different in the absence of expulsion, which corresponds to the region below the threshold.

4.4 Validation by edge and gap affected welding points

Two more cases have been considered to validate the proposed index: initial gap (IG) and edge proximity (EP) (Figure 8). All welding points have been performed

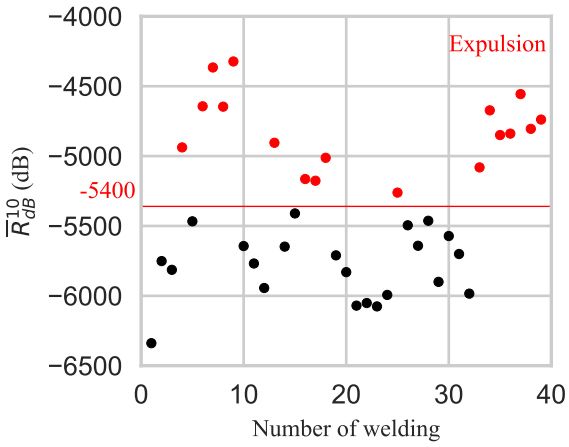

(a) $\overline{R}^{10}_{\mathrm{dB}}$ values for samples 1-39.

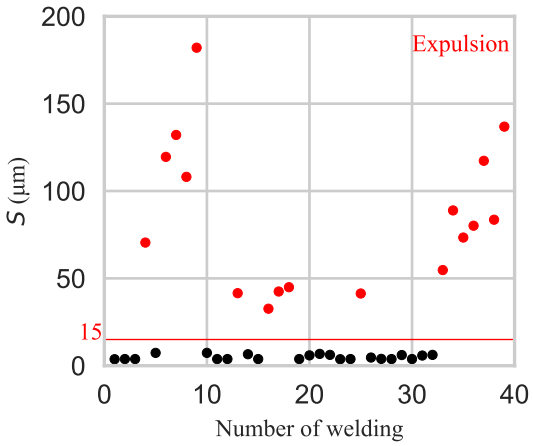

(b) S values for samples 1-39.

Fig. 7: $\overline{R}^{10}_{\mathrm{dB}}$ and S values for samples 1-39. Joints with and without expulsions are denoted in red and black, respectively. The horizontal red line denotes the identified threshold, splitting joints with and without expulsions.

with $I = 7$ kA and P=1 bar (see Table 1). Firstly, 3 samples have been made without any disturbance. Then, for each gap condition $IG = \{0.7, 1, 1.3\}$ mm, 3 samples have been performed. The same has been done for the edge proximity, considering $EP = \{10, 5, 0\}$ mm. The validation set contains 21 samples.
All weldments done in abnormal conditions (IG and EP) have been affected by expulsion. Figure 9 shows the differences of the acquired forces for specimens with IG1.3

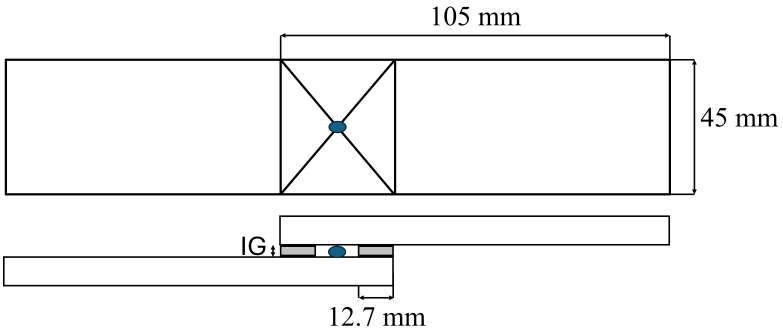

(a) Initial gap welding geometry with $IG = \{0.7, 1, 1.3\}$ mm.

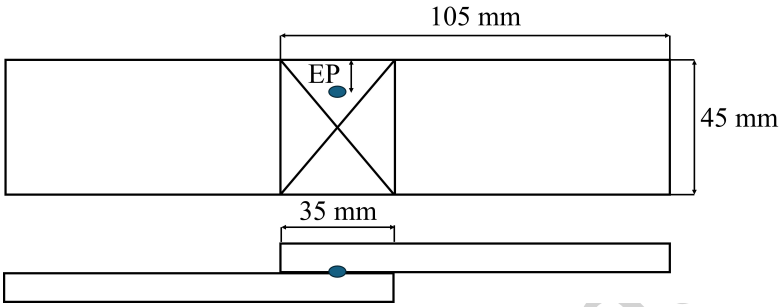

(b) Edge proximity welding geometry with $EP = \{10, 5, 0\}$ mm.

Fig. 8: Initial gap and edge welding geometry.

and EP10 conditions compared to a normal weldment having group 1 parameters. Even in this case, $\overline{X}_{\mathrm{dB}}(n)$ is higher for the expulsion-affected points.

Following the procedure previously discussed, $\overline{R}^{10}_{\mathrm{dB}}$ and S have been computed to validate the proposed approach. Figure 10 shows the indexes for the validation set, demonstrating that the thresholds identified in the previous paragraph are valid even in considered IG and EP cases. Indeed, the IG disturbance reduces the initial contact area between the sheets, resulting in a rapid temperature increase and expulsions. In the presence of EP welding, expulsion occurs since a lower heat dissipation leads to a rapid temperature rise in the welding. It can be observed that increasing the gap, $\overline{R}^{10}_{\mathrm{dB}}$ increases since the process becomes unstable. The same can be noted for edge weldments: moving from EP10 to EP0, $\overline{R}^{10}_{\mathrm{dB}}$ decreases due to less vibrations during welding. The lack of surrounding cold metal allows the expansion of the nugget, reducing the internal pressure and, thereby, lowering the likelihood of expulsion formation[21, 43, 44].

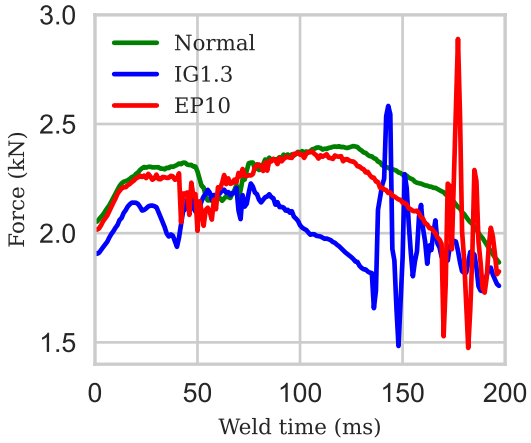

(a) Force behavior for normal and abnormal conditions.

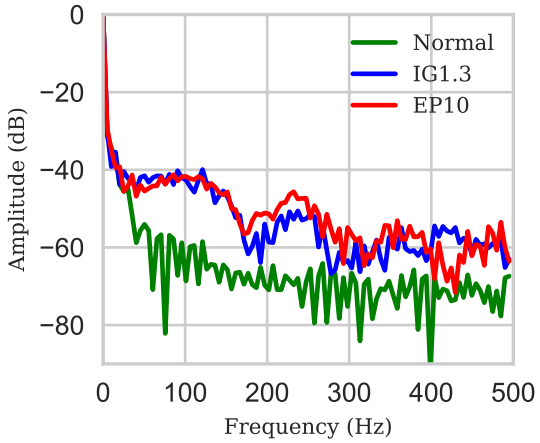

(b) Force energy spectral density for normal and abnormal conditions.

Fig. 9: Force and energy density for normal, IG1.3 and EP10 specimens.

4.5 Comparison of residual energy with displacement signal to detect expulsiones

Figure 11 compares all 60 indexes S and $\overline{R}^{10}_{\mathrm{dB}}$ to highlight their sensitivity in expulsions detection, where $\overline{R}^{10}_{\mathrm{dB}}$ is shown as a function of S. Given the previously defined threshold values on S and $\overline{R}^{10}_{\mathrm{dB}}$, the set of joints with expulsions is all contained within the upper right plane, while the lower left plane has the joints without expulsions. Displacement- and force-based expulsion indexes are proportional in the case of expulsions. They grow as the welding conditions are far from the optimal one identified

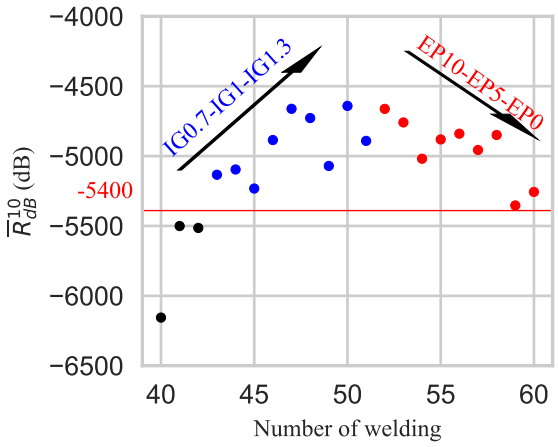

(a) $\overline{R}^{10}_{\mathrm{dB}}$ values and the trend for validation set weld joints.

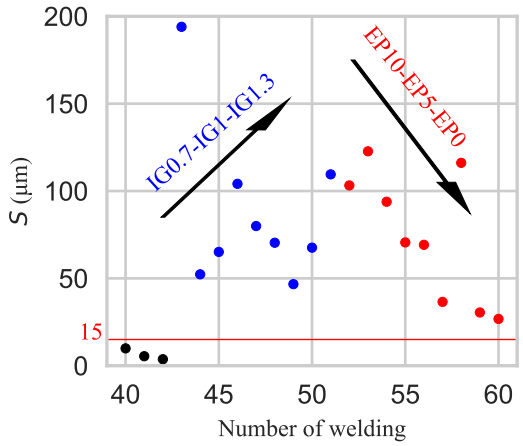

(b) S values and the trend for validation set weld joints.

Fig. 10: $\overline{R}^{10}_{\mathrm{dB}}$ and S values for validation set weld joints (numbers 40-60). The horizontal red line denotes the identified threshold, splitting joints with and without expulsions.

in the lobe diagram (Figure 5). However, for joints without expulsions, the values of S are all close to each other, around 5 µm. In this case, $\overline{R}^{10}_{\mathrm{dB}}$ shows large variability based on the welding parameters, getting close to the threshold when the weldings are moving toward the expulsion conditions. Thus, the online monitoring of $\overline{R}^{10}_{\mathrm{dB}}$ can

Table 1: Experimental input parameters. I is welding current, P is electrode pressure. The validation set has 21 out of 60 samples.

Group ID / set	I (kA)	P (bar)
1	7.0	1.0
2	7.5	1.0
3	8.0	1.0
4	6.5	1.0
5	6.5	0.8
6	7.0	0.8
7	6.5	1.1
8	7.0	1.1
9	7.5	1.1
10	6.5	0.9
11	7.0	0.9
12	7.5	0.9
13	8.0	1.1
validation	7.0	1.0

help working close to the extreme conditions in the lobe diagram, close to the spatter condition. The index trend, possibly due to electrode wear, can be monitored and signaled to the user when it approaches the threshold value, preventing expulsions.

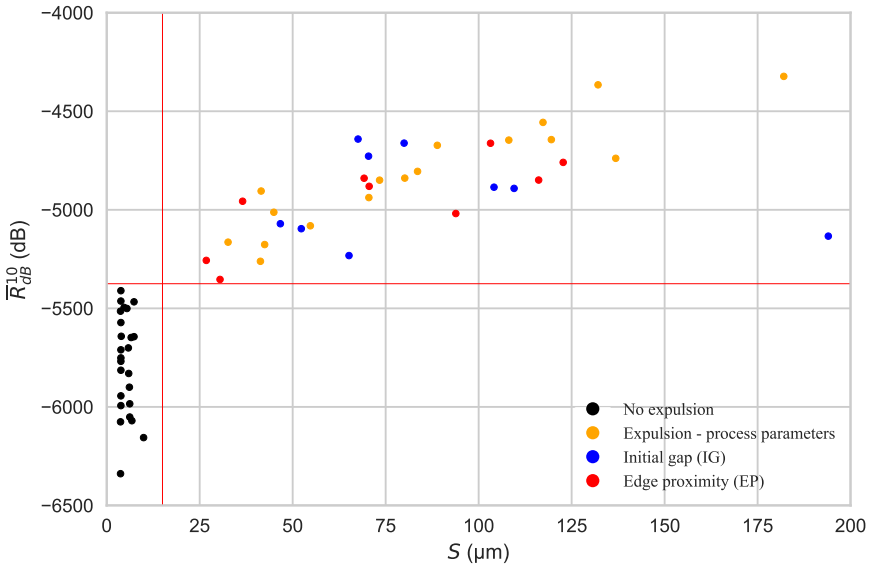

Fig. 11: $\overline{R}^{10}_{\mathrm{dB}}$ vs S. The red lines denote the identified thresholds, splitting joints with and without expulsions. All the weldments not affected by expulsion have S between lower than 15 µm and $\overline{R}^{10}_{\mathrm{dB}}$ lower than -5400 dB.

5 Conclusion

This work proposes an expulsion presence-related index, $\overline{R}^{10}_{\mathrm{dB}}$, capable of recognizing expulsion and its intensity level. In total, 60 welding points, in different conditions, have been performed.

First, an experimental campaign has been conducted following the corresponding ISO standards to identify process parameters that lead to expulsion thanks to the weldability lobe construction. Frequency domain analysis of the extracted force signal has been exploited to build the index. The validity of the proposed index, in terms of binary expulsion identification, has been verified using another index constructed from the electrode displacement. Such a signal is widely used in the literature when dealing with expulsion recognition. However, a different behavior has been noticed when the process works in standards-conforming situations.

Second, another campaign was done to validate the ability of the proposed index to recognize expulsion in abnormal conditions: initial gap and edge proximity. For each condition, 3 replicas for 3 different levels have been made. Even in this case, the proposed $\overline{R}^{10}_{\mathrm{dB}}$ index was capable of catching the expulsion phenomenon.

The main findings of this study are:

21

- As the displacement-related index, S, the $\overline{R}^{10}_{\mathrm{dB}}$ expulsion indicator can always recognise expulsion. Consequently, both signals can be used for binary expulsion classification, reaching 100% accuracy.
- Although the physical amount of expulsion has not been measured, it has been shown that $\overline{R}^{10}_{\mathrm{dB}}$ is capable of quantifying the level of the spatter. It has been demonstrated that welding points with higher expulsion intensity (i.e., bottom right area of the weldability lobe) have a higher $\overline{R}^{10}_{\mathrm{dB}}$.
- Regarding induced expulsion by extreme process parameters, significant differences exist when the process works under the expulsion border. The $\overline{R}^{10}_{\mathrm{dB}}$ demonstrates a higher sensitivity in catching near-expulsion working conditions. It can identify boundary conditions characterized by a high heat input, leading to a large weld diameter and a higher probability of expulsion occurrence. Therefore, $\overline{R}^{10}_{\mathrm{dB}}$ not only can distinguish between non-expulsion and expulsion but it can quantify expulsion intensity and how far, based on the actual working conditions, the process is from the expulsion limit.
- Initial gap and edge proximity conditions leading to expulsion can be automatically recognized. In particular, the $\overline{R}^{10}_{\mathrm{dB}}$ index can identify the relationship between the expulsion intensity and the severity of the disturbance. For example, a higher gap implies a higher $\overline{R}^{10}_{\mathrm{dB}}$.

The proposed index enhances RSW process monitoring for achieving the following:

- Recognition and quantification of expulsion, being undesirable and unacceptable for RSW standards.
- Identification of any shift or trends leading to expulsion and intervention before expulsion arises.
- Detection of spatter deriving from abnormal conditions as initial gap and edge proximity.

Future works could focus on the combination of the $\overline{R}^{10}_{\mathrm{dB}}$ with other techniques that are capable of distinguishing the different causes of expulsion (e.g., wrong process parameters, electrode wear, initial gap, edge proximity, electrode-sheet inclination).

Acknowledgements

This study was supported by J-Tech@PoliTo, advanced joining technologies research center at Politecnico di Torino. The authors thank Mr Matteo Perrone for his help and assistance during the experimental campaign.

Declarations

Funding. Not applicable.

Competing interests. Not applicable.

Authors' contribution. All the authors contributed equally to the work.

References

[1] H. Wang, Y. Zhang, G. Chen, Resistance spot welding processing monitoring based on electrode displacement curve using moving range chart. Measurement: Journal of the International Measurement Confederation **42**(7), 1032 – 1038 (2009). https://doi.org/10.1016/j.measurement.2009.03.005

[2] D. Zhao, N. Vdonin, M. Slobodyan, S. Butsykin, A. Kiselev, A. Gordynets, Y. Wang, Dynamic resistance signal–based wear monitoring of resistance spot welding electrodes. International Journal of Advanced Manufacturing Technology **133**(7-8), 3267 – 3281 (2024). https://doi.org/10.1007/s00170-024-13993-y

[3] S. Chen, T. Sun, X. Jiang, J. Qi, R. Zeng, Online monitoring and evaluation of the weld quality of resistance spot welded titanium alloy. Journal of Manufacturing Processes **23**, 183–191 (2016). https://doi.org/10.1016/j.jmapro.2016.06.003

[4] W. Dai, D. Li, Y. Zheng, D. Wang, D. Tang, H. Wang, Y. Peng, Online quality inspection of resistance spot welding for automotive production lines. Journal of Manufacturing Systems **63**, 354–369 (2022). https://doi.org/10.1016/j.jmsy.2022.04.008

[5] L. Santoro, V. Razza, M. De Maddis, Frequency-based analysis of active laser thermography for spot weld quality assessment. International Journal of Advanced Manufacturing Technology **130**(5-6), 3017 – 3029 (2024). https://doi.org/10.1007/s00170-023-12845-5

[6] J. Lee, I. Noh, S.I. Jeong, Y. Lee, S.W. Lee, Development of Real-time Diagnosis Framework for Angular Misalignment of Robot Spot-welding System Based on Machine Learning. Procedia Manufacturing **48**, 1009–1019 (2020). https://doi.org/10.1016/j.promfg.2020.05.140

[7] P. Podržaj, I. Polajnar, J. Diaci, Z. Kari, Expulsion detection system for resistance spot welding based on a neural network. Measurement Science and Technology **15**(3), 592–598 (2004). https://doi.org/10.1088/0957-0233/15/3/011

[8] L. Panza, G. Bruno, M. De Maddis, F. Lombardi, P. Russo Spena, E. Traini, Data-Driven Framework for Electrode Wear Prediction in Resistance Spot Welding. IFIP International Conference on Product Lifecycle Management (2022). https://doi.org/{10.1007/978-3-030-94335-6_17}

[9] J. Kershaw, H. Ghassemi-Armaki, B.E. Carlson, P. Wang, Advanced process characterization and machine learning-based correlations between interdiffusion layer and expulsion in spot welding. Journal of Manufacturing Processes **109**, 222 – 234 (2024). https://doi.org/10.1016/j.jmapro.2023.12.013

[10] L. Santoro, V. Razza, M. De Maddis, Nugget and corona bond size measurement through active thermography and transfer learning model. International Journal of Advanced Manufacturing Technology **133**(11-12), 5883 – 5896 (2024). https://doi.org/10.1007/s00170-024-14096-4

[11] Y.J. Xia, Z.W. Su, Y.B. Li, L. Zhou, Y. Shen, Online quantitative evaluation of expulsion in resistance spot welding. Journal of Manufacturing Processes **46**, 34–43 (2019). https://doi.org/10.1016/j.jmapro.2019.08.004

[12] L. Yi, W. Rui, X. Xiaojian, Z. Yang, Expulsion analysis of resistance spot welding on zinc-coated steel by detection of structure-borne acoustic emission signals. International Journal of Advanced Manufacturing Technology **84**(9-12), 1995 –

23

2002 (2016). https://doi.org/10.1007/s00170-015-7846-z

[13] M. Ullrich, M. Wohner, S. Jüttner, Quality monitoring for a resistance spot weld process of galvanized dual-phase steel based on the electrode displacement. Welding in the World **68**(7), 1791 – 1800 (2024). https://doi.org/10.1007/s40194-024-01720-w

[14] B. Xing, Y. Xiao, Q.H. Qin, H. Cui, Quality assessment of resistance spot welding process based on dynamic resistance signal and random forest based. International Journal of Advanced Manufacturing Technology **94**(1-4), 327 – 339 (2018). https://doi.org/10.1007/s00170-017-0889-6

[15] Y. Ma, P. Wu, C. Xuan, Y. Zhang, H. Su, Review on Techniques for On-Line Monitoring of Resistance Spot Welding Process. Advances in Materials Science and Engineering **2013**, 1–6 (2013). https://doi.org/10.1155/2013/630984

[16] C. Ma, S.D. Bhole, D.L. Chen, A. Lee, E. Biro, G. Boudreau, Expulsion monitoring in spot welded advanced high strength automotive steels. Science and Technology of Welding and Joining **11**(4), 480–487 (2006). https://doi.org/10.1179/174329306X120895

[17] BS EN ISO 17677-1-2021 - Resistance welding. Vocabulary. Part 1, Spot, projection and seam welding (2021)

[18] H. Zhang, J. Senkara, *Resistance Welding - Fundamentals and Applications*, 2nd edn. (2011). https://doi.org/10.1201/b11752

[19] M. Pouranvari, A. Abedi, P. Marashi, M. Goodarzi, Effect of expulsion on peak load and energy absorption of low carbon steel resistance spot welds. Science and Technology of Welding and Joining **13**(1), 39–43 (2008). https://doi.org/10.1179/174329307X249342

[20] Y. Shen, Y.J. Xia, H. Li, L. Zhou, Y.B. Li, H.T. Pan, A Novel Expulsion Control Strategy With Abnormal Condition Adaptability for Resistance Spot Welding. Journal of Manufacturing Science and Engineering **143**(11), 111009 (2021). https://doi.org/10.1115/1.4051011

[21] Y.J. Xia, Z. Li, W. Wang, T. Yang, G. Pi, Y. Li, Influence mechanism of initial gap disturbance on the resistance spot welding process. Automotive Innovation **7**(2), 360 – 372 (2024). https://doi.org/10.1007/s42154-023-00264-x

[22] D.F. Farson, J.Z. Chen, K. Ely, T. Frech, Monitoring of expulsion in small scale resistance spot welding. Science and Technology of Welding and Joining **8**(6), 431–436 (2003). https://doi.org/10.1179/136217103225009071

[23] Z. Mikno, A. Pilarczyk, M. Korzeniowski, P. Kustroń, A. Ambroziak, Analysis of resistance welding processes and expulsion of liquid metal from the weld nugget. Archives of Civil and Mechanical Engineering **18**(2), 522–531 (2018). https://doi.org/10.1016/j.acme.2017.08.003

[24] Q. Fan, G. Xu, X. Gu, Expulsion characterization of stainless steel resistance spot welding based on dynamic resistance signal. Journal of Materials Processing Technology **236**, 235–240 (2016). https://doi.org/10.1016/j.jmatprotec.2016.05.026

[25] S. Kim, I. Hwang, D.Y. Kim, Y.M. Kim, M. Kang, J. Yu, Weld-Quality Prediction Algorithm Based on Multiple Models Using Process Signals in Resistance Spot Welding. Metals **11**(9), 1459 (2021). https://doi.org/10.3390/met11091459

24

[26] L. Zhou, T. Zhang, Z. Zhang, Z. Lei, S. Zhu, Monitoring of resistance spot welding expulsion based on machine learning. Science and Technology of Welding and Joining **27**(4), 292–300 (2022). https://doi.org/10.1080/13621718.2022.2051408

[27] M. Russell, J. Kershaw, Y. Xia, T. Lv, Y. Li, H. Ghassemi-Armaki, B.E. Carlson, P. Wang, Comparison and explanation of data-driven modeling for weld quality prediction in resistance spot welding. Journal of Intelligent Manufacturing (2023). https://doi.org/10.1007/s10845-023-02108-1

[28] W. Yang, P. P Gao, X. Gao, Online evaluation of resistance spot welding quality and defect classification. Measurement Science and Technology **34**(9) (2023). https://doi.org/10.1088/1361-6501/acce58

[29] J.U. Choi, S.H. Park, Quality monitoring solution: measurement and modeling of product external diameter in cnc turning. International Journal of Advanced Manufacturing Technology **133**(9-10), 4195 – 4203 (2024). https://doi.org/10.1007/s00170-024-13962-5

[30] B. Bevans, A. Ramalho, Z. Smoqi, A. Gaikwad, T.G. Santos, P. Rao, J. Oliveira, Monitoring and flaw detection during wire-based directed energy deposition using in-situ acoustic sensing and wavelet graph signal analysis. Materials & Design **225**, 111480 (2023). https://doi.org/https://doi.org/10.1016/j.matdes.2022.111480

[31] J. Petrich, R.W. Smith, E.T.W. Reutzel, Acoustic laser triangulation and tagging for additive manufacturing process monitoring. International Journal of Advanced Manufacturing Technology **129**(7-8), 3233 – 3245 (2023). https://doi.org/10.1007/s00170-023-12408-8

[32] D. Gauder, M. Biehler, J. Gölz, V. Schulze, G. Lanza, In-process acoustic pore detection in milling using deep learning. CIRP Journal of Manufacturing Science and Technology **37**, 125–133 (2022). https://doi.org/https://doi.org/10.1016/j.cirpj.2022.01.008. URL https://www.sciencedirect.com/science/article/pii/S1755581722000141

[33] N. Wu, S. Chen, J. Xiao, Wavelet analysis-based expulsion identification in electrode force sensing of resistance spot welding. Welding in the World **62**(4), 729–736 (2018). https://doi.org/10.1007/s40194-018-0594-6

[34] S. Chen, N. Wu, J. Xiao, T. Li, Z. Lu, Expulsion Identification in Resistance Spot Welding by Electrode Force Sensing Based on Wavelet Decomposition with Multi-Indexes and BP Neural Networks. Applied Sciences **9**(19), 4028 (2019). https://doi.org/10.3390/app9194028

[35] L. Panza, M. De Maddis, P. Russo Spena, Use of electrode displacement signals for electrode degradation assessment in resistance spot welding. Journal of Manufacturing Processes **76**, 93–105 (2022). https://doi.org/10.1016/j.jmapro.2022.01.060

[36] L. Panza, G. Bruno, G. Antal, M. De Maddis, P. Russo Spena, Machine learning tool for the prediction of electrode wear effect on the quality of resistance spot welds. International Journal on Interactive Design and Manufacturing (IJIDeM) (2024). https://doi.org/10.1007/s12008-023-01733-7

[37] R.L. Allen, D.W. Mills, *Signal Analysis: Time, Frequency, Scale, and Structure* (John Wiley & Sons, 2004). https://doi.org/10.1002/047166037X

25

[38] K. Zhou, L. Cai, Online nugget diameter control system for resistance spot welding. International Journal of Advanced Manufacturing Technology **68**(9-12), 2571 – 2588 (2013). https://doi.org/10.1007/s00170-013-4886-0

[39] BS EN ISO 14273-2016-Resistance welding. Destructive testing of welds. Specimen dimensions and procedure for tensile shear testing resistance spot and embossed projection welds (2016)

[40] BS EN ISO 14373-2015-Resistance welding. Procedure for spot welding of uncoated and coated low carbon steels (2015)

[41] BS EN ISO 14327-2004-Resistance welding. Procedures for determining the weldability lobe for resistance spot, projection and seam welding (2004)

[42] BS EN ISO 18278-1-2022-Resistance welding. Weldability. Part 1, General requirements for the evaluation of weldability for resistance spot, seam and projection welding of metallic materials (2022)

[43] X. Wang, Y. Li, G. Meng, Monitoring of resistance spot weld quality using electrode vibration signals. Measurement Science and Technology **22**(4) (2011). https://doi.org/10.1088/0957-0233/22/4/045705

[44] Y.J. Xia, L. Zhou, Y. Shen, D.M. Wegner, A.S. Haselhuhn, Y.B. Li, B.E. Carlson, Online measurement of weld penetration in robotic resistance spot welding using electrode displacement signals. Measurement: Journal of the International Measurement Confederation **168** (2021). https://doi.org/10.1016/j.measurement.2020.108397

26